ISSN 1063-7761, Journal of Experimental and Theoretical Physics, 2019, Vol. 129, No. 1, pp. 112–115. © Pleiades Publishing, Inc., 2019.
Russian Text © The Author(s), 2019, published in Zhurnal Eksperimental'noi i Teoreticheskoi Fiziki, 2019, Vol. 156, No. 1, pp. 135–139.

ORDER, DISORDER, AND PHASE TRANSITION IN CONDENSED SYSTEM

Magnetic and Resistive Properties of Magnetite/Iridate Heterostructures

T. A. Shaikhulov[a,*], G. A. Ovsyannikov[a], V. V. Demidov[a], and N. V. Andreev[b]

[a] *Kotel'nikov Institute of Radio Engineering and Electronics, Russian Academy of Sciences, Moscow, 125009 Russia*

[b] *National University of Science and Technology MISiS, Moscow, 119991 Russia*

**e-mail: shcaihulov@hitech.cplire.ru*

Received January 14, 2019; revised February 21, 2019; accepted February 22, 2019

Abstract—A technique is developed to grow epitaxial heterostructures consisting of strontium iridate ($SrIrO_3$) and lanthanum–strontium manganite ($La_{0.7}Sr_{0.3}MnO_3$). Their transport properties and ferromagnetic resonance spectra are measured. The parameters obtained are compared with the properties of individual iridate and manganite films. The results of resistive measurements point to conduction of the iridate/manganite interface. As temperature decreases, the ferromagnetic resonance line width increases and the resonance field decreases, which indicates the appearance of additional ferromagnetic ordering in the heterostructures.

DOI: 10.1134/S1063776119060153

1. INTRODUCTION

The 3*d*-transmission metal oxides (TMOs) have various functional properties, which are caused by a strong electron–electron correlation. However, the spin–orbit interaction in 3*d*-TMOs is usually weak [1]. A well-pronounced spin–orbit interaction has recently attracted attention due to the appearance of new toplogical states [2–5] and spintronics [6, 7]. The contact between 3*d*- and 5*d*-TMOs creates a unique interface, where these fundamental phenomena can exist and interact. Breaks in topological symmetry and a gap in an excitation spectrum at the 5*d*-TMO/ferromagnet interface can appear, which can cause strong magnetoelectric effects [8, 9]. In this paper, we present the results of the growth of an epitaxial heterostructure from ferromagnetic manganite and paramagnetic iridate, which have a strong spin–orbit interaction, and measure their electrophysical and magnetic properties.

The heterostructures were grown by magnetron sputtering onto a (110) single-crystal neodymium gallate $NdGaO_3$ (NGO) substrate at a temperature T = 820°C and an oxygen pressure of 0.7 mbar for the $La_{0.7}Sr_{0.3}MnO_3$ (LSMO) manganite [10] and T = 770°C and a pressure of 0.3 mbar for the $SrIrO_3$ (SIO) iridate [11]. The manganite film thickness was varied from 5 to 10 nm. The crystal structures of the heterostructures were analyzed by X-ray diffraction (XRD).

2. CRYSTALLOGRAPHIC STRUCTURE

Figure 1 shows the $2\theta/\omega$ X-ray diffraction pattern of the SIO/LSMO grown on a (110)NGO substrate. The structure and the lattice parameters were determined from the peak positions. The SIO film was found to have the orthorhombic *Pnma* modification with lattice parameters a = 0.55909 nm, b = 0.78821 nm, and c = 0.55617 nm, and this structure can be approximately considered as a pseudocube with a parameter a = 0.398 nm. The structure of the LSMO is taken to be pseudocubic with a parameter a = 0.389 nm. The X-ray diffraction pattern has multiple reflections from the (001)SIO and (001)LSMO heterostructure planes and reflections from the (110)NGO substrate. Therefore, we conclude that the heterostructure layers grew in a cube-on-cube manner with the epitaxial relations

$$(001)\text{SIO} \parallel (001)\text{LSMO} \parallel (110)\text{NGO},$$

$$[100]\text{SIO} \parallel [100]\text{LSMO} \parallel [001]\text{NGO}.$$

The interplanar spacing in the LSMO film remained almost unchanged in the heterostructure (0.388 nm). The interplanar spacing in the SIO film is 0.403 nm in the individual film and 0.404 nm in the heterostructure. The inset to Fig. 1 shows the rocking curve of the (002) reflection of the SIO heterostructure. A narrow rocking curve (curve width $\Delta\omega = 0.07°$) indicate a high quality of the layers. The increase in the lattice param-

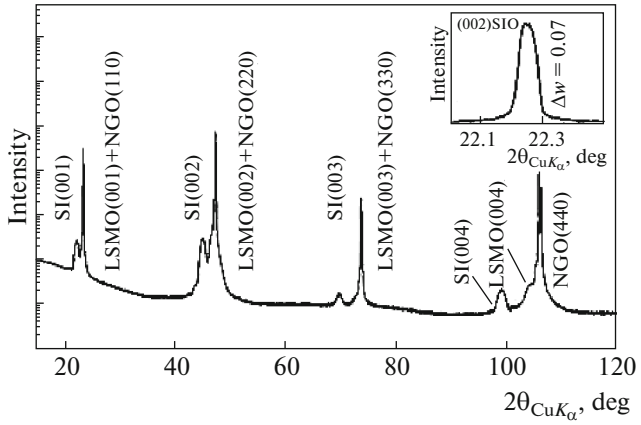

Fig. 1. 2θ/ω X-ray diffraction pattern of Bregg's reflection SIO/LSMO heterostructure grown on a (110)NGO substrate. The (002)SIO Δω is shown in the inset (Δω is the rocking curve width).

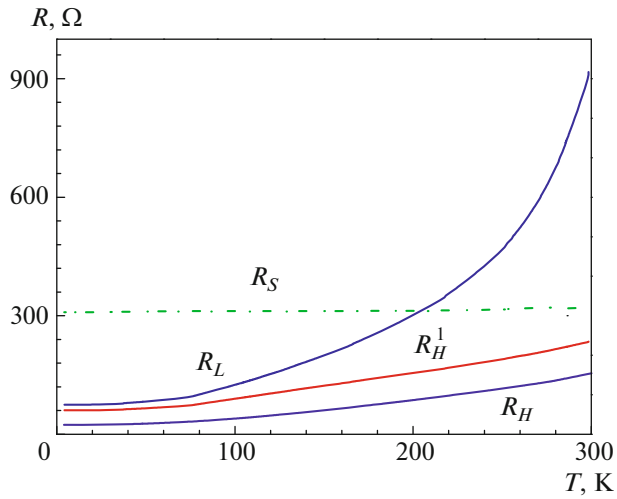

Fig. 2. (Color online) Temperature dependences of the resistances of individual 10-nm-thick SIO (R_S) and 12-nm-thick LSMO (R_L) films and the SIO/LSMO heterostructure (R_H) with SIO and LSMO films of the same thicknesses. R_H^1 is the temperature dependence obtained from the resistances of the individual films connected in parallel.

eter in the direction normal to the substrate surface is likely to be related to the stresses in the SIO film that appear during its epitaxial growth. The X-ray diffraction patterns were recorded at room temperature.

3. ELECTRIC TRANSPORT PARAMETERS OF THE FILMS AND HETEROSTRUCTURES

The electrical properties of the heterostructure films were measured by the four-point probe method in the substrate plane. The temperature dependences of electrical resistance were measured to compare the current passing in the films and the heterostructure (Fig. 2). Figure 2 also shows the resistance that is equal to the resistances of the upper SIO film (R_S) and the lower LSMO film (R_L) connected in parallel, $R_H^1 = R_S R_L/(R_L + R_S)$. R_H^1 is seen to exceed the measured resistance of the entire heterostructure (R_H). Therefore, it is necessary to take into account the interface resistance $R_I = R_H^1 R_H/(R^1 - R_H)$, which is connected in parallel to the resistances of the films.

Figure 3 shows the temperature dependences of interface resistance R_I for the interfaces of the heterostructures SIO/LSMO/NGO, LSMO/SIO/NGO, and Pt/LSMO/NGO. R_I is seen to depend on both the material of the film and the sequence of film growth. At a low temperature, the electrical resistivity of the SIO/LSMO interface is $\rho_I = 5 \times 10^{-6}$ Ω cm on the assumption that its thickness is 1 nm. Such a low electrical resistivity of the interface points to the possibility of existence of a two-dimensional high-mobility electron gas [12, 13].

TMOs differ substantially from conventional metal oxides because of the presence of strong electron–electron correlations. A large number of degrees of freedom, namely, spin, charge, lattice, and orbital degrees, in them leads to complex behavior of these materials, especially at the interface. The charge transport at the heterostructure interface differs substantially from that in both individual films and simple metals [12, 13].

4. FERROMAGNETIC RESONANCE IN THE HETEROSTRUCTURE

Figure 4 presents the ferromagnetic resonance (FMR) spectra of an individual LSMO film and two SIO/LSMO heterostructures with different film thicknesses. The measurements were carried out on a standard ER 200 (Bruker) spectrometer at a frequency of 9.2 GHz and a temperature $T = 294$ K. The external magnetic vector was always in the sample plane (so-called in-plane orientation). All three spectra are shown for the case where an external magnetic field is applied along the easy axis of in-plane uniaxial magnetic anisotropy [10].

The strontium iridate SIO film under study is known to be paramagnetic [14]. The sensitivity of our spectrometer did not allow us to detect the paramagnetic resonance signal from a 10-nm-thick SIO film; therefore, the spectra presented in Fig. 4 belong to the ferromagnetic resonance (FMR) of the LSMO manganite in the SIO/LSMO heterostructure. The FMR spectrum of the SIO/LSMO heterostructure with a 12-nm-thick LSMO film is seen to resemble that of the individual film: the resonance fields and, hence, the magnetizations are close, and signal width of the SIO/LSMO heterostructure is only slightly larger than

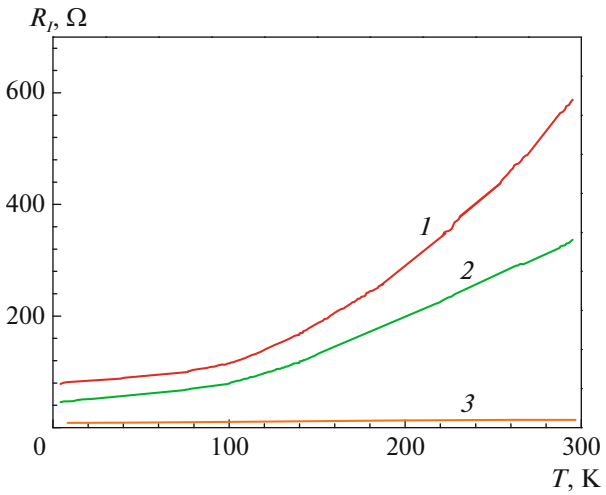

Fig. 3. (Color online) Temperature dependences of the resistances R_I of the interfaces in heterostructures (*1*) LSMO(15 nm)/SIO(10 nm), (*2*) SIO(10 nm)/LSMO(12 nm), and (*3*) Pt(10 nm)/LSMO(20 nm).

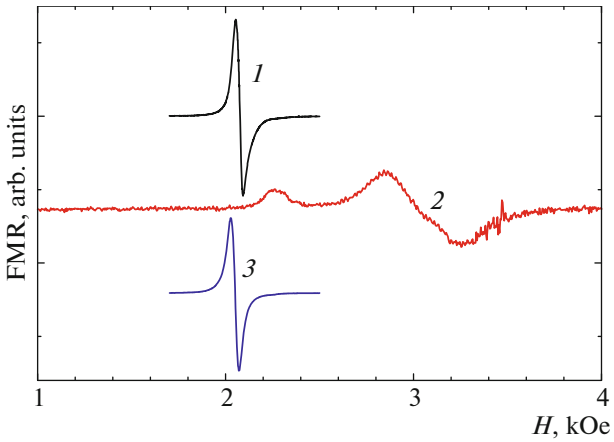

Fig. 4. (Color online) FMR spectra of (*1*) individual 15-nm-thick LSMO film and two SIO/LSMO heterostructures with LSMO film (*2*) 3.5 and (*3*) 12 nm thick and a 10-nm-thick SIO film. $T = 294$ K.

that of the individual film. The increase in the FMR line width can be explained by both the additional relaxation caused by the spin current in a ferromagnet/normal metal structure and the additional inhomogeneity of the spin system in the SIO/LSMO structure as compared to the individual LSMO film. However, the signal of the SIO/LSMO structure with a 3.5-nm-thick LSMO film differs significantly from the FMR line of the individual film. First, it is detected in higher fields, which points to a lower magnetization of the spin system in this structure. Second, this signal has a significantly larger width and exhibits the presence of at least two spin subsystems. When the temperature decreases, the spectrum of the SIO/LSMO heterostructure with a 3.5-nm-thick LSMO film is represented by one line, which demonstrates that we deal with one system of ordered spins the magnetization of which becomes more homogeneous with decreasing temperature. As a result, we obtained the temperature dependence of the resonance field for both SIO/LSMO heterostructures under study.

Figure 5 shows the resonance fields of the two heterostructures obtained when an external magnetic field is applied along the hard axis of in-plane uniaxial magnetic anisotropy. This direction of an external magnetic field was chosen from the condition of the minimum contribution of magnetic anisotropy in the resonance ratio for FMR [10]. Thus, we think that the obtained temperature dependence characterizes the change in the magnetization of the sample. In this approximation, we can state that the decrease in the resonance field is caused by an increase in the magnetization of the sample.

As follows from an analysis of the temperature dependences of resonance field H_0, the Curie temperature of the structure with a 3.5-nm-thick LSMO film is slightly higher than 300 K (Fig. 5). The Curie temperature of LSMO/SIO with a 10-nm-thick LSMO film is significantly higher (340–350 K), which is typical of the individual LSMO film on an NGO substrate. Note that a decrease in the Curie temperature of a thin film with decreasing film thickness is a well-known effect. The sharp decrease in H_0 in both structures when temperature decreases below 50 K raises a significantly larger number of questions. This decrease cannot be explained by a sharp increase in the magnetization of the LSMO layer, since this assumption is in conflict with the measurements of individual LSMO films. As the temperature decreases, the $H_0(T)$ dependence is usually saturated at temperatures below 100 K. The SIO film is likely to affect the FMR spectrum of the LSMO film. An analogous increase in the magnetization of the LSMO layer in a bilayer LSMO/SRO/NGO (here, SRO = $SrRuO_3$) structure [14] at temperatures below 150 K was detected in [15]. That effect was caused by the appearance of an interlayer exchange coupling after the SRO layer transformed into a ferromagnetic state [16]. The appearance of ferromagnetism in a thin SIO layer was observed in the following SIO-containing superlattices: $(SrMnO_3/SIO)_n$ [17], $(SrTiO_3/SIO)_n$ [18], and $(LSMO/SIO)_n$ [19, 20]. The SIO film is assumed to transform into a ferromagnetic state near 50 K. The interlayer exchange coupling of two ferromagnets causes a sharp decrease in the resonance field. The exact magnetization of the LSMO film with allowance for the influence of magnetic anisotropy can be determined by measuring angular dependences of its FMR spectra at various temperatures.

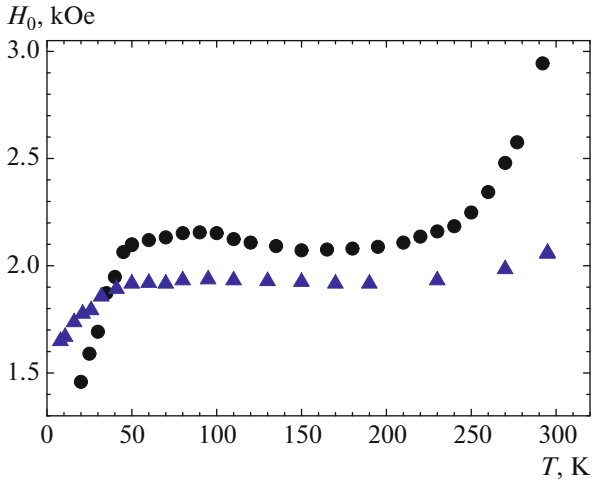

Fig. 5. (Color online) Temperature dependences of the resonance field for two SIO/LSMO heterostructures with manganite films of 3.5 nm (circles) and 12 nm (triangles) with a SIO film thickness of 10 nm.

5. CONCLUSIONS

The measurements of the transport and magnetic properties of epitaxial $SrIrO_3/La_{0.7}Sr_{0.3}MnO_3$ heterostructures revealed unusual properties of the interface in them. The measurement results point to the presence of a conduction channel at the iridate/manganite interface and to possible appearance of ferromagnetism at the SIO/LSMO interface at a temperature below 50 K.

ACKNOWLEDGMENTS

We thank V.A. Atsarkin, A.L. Klimov, A.M. Petrzhik, and T.A. Sviridova for useful discussions and their help in the experiments.

FUNDING

This work was performed under State assignment and supported in part by the Russian Foundation for Basic Research, project nos. 19-07-00143 and 17-02-00145.

ADDITIONAL INFORMATION

This work was based on our report for the XXXVIII Conference on Low-Temperature Physics (NT-38).

REFERENCES

1. N. G. Bebenin, R. I. Zainullina, and V. V. Ustinov, Phys. Usp. **61**, 719 (2018).
2. L. Zhang, B. Pang, Y. B. Chen, and Y. Chen, Crit. Rev. Sol. St. Mater. Sci. **43**, 367 (2018).
3. D. Pesin and L. Balents, Nat. Phys. **6**, 376 (2010).
4. F. Wang and T. Senthil, Phys. Rev. Lett. **106**, 136402 (2011).
5. D. Xiao, W. Zhu, Y. Ran, et al., Nat. Commun. **2**, 596 (2011).
6. T. Seki, Yu. Hasegawa, S. Mitani, et al., Nat. Mater. **7**, 125 (2008).
7. E. Saitoh, M. Ueda, H. Miyajima, and G. Tatara, Appl. Phys. Lett. **88**, 182509 (2006).
8. X. L. Qi, T. L. Hughes, and S. C. Zhang, Phys. Rev. B **78**, 95424 (2008).
9. A. Manchon, H. C. Koo, J. Nitta, et al., Nat. Mater. **14**, 871 (2015).
10. V. V. Demidov, I. V. Borisenko, A. A. Klimov, G. A. Ovsyannikov, A. M. Petrzhik, and S. A. Nikitov, J. Exp. Theor. Phys. **112**, 825 (2011).
11. Yu. V. Kislinskii, G. A. Ovsyannikov, A. M. Petrzhik, K. Y. Constantinian, N. V. Andreev, and T. A. Sviridova, Phys. Solid State **57**, 2519 (2015).
12. E. Dagotto, Science (Washington, DC, U. S.) **309**, 257 (2005).
13. S. Thiel, G. Hammer, A. Schmehl, et al., Science (Washington, DC, U. S.) **313**, 1942 (2006).
14. M. Longo, J. A. Kafalas, and R. J. Arnott, J. Solid State Chem. **3**, 174 (1971).
15. V. V. Demidov and G. A. Ovsyannikov, J. Appl. Phys. **122**, 013902 (2017).
16. N. M. Kreines, D. I. Kholin, and S. O. Demokritov, J. Low Temp. Phys. **38**, 826 (2012).
17. J. Nichols, X. Gao, S. Lee, et al., Nat. Commun. **7**, 12721 (2016).
18. Di Yi, C. L. Flint, and P. P. Balakrishnan, Phys. Rev. Lett. **119**, 077201 (2017).
19. D. Yi, J. Liu, Sh.-L. Hsu, L. Zhang, et al., Proc. Nat. Acad. Sci. **113**, 6397 (2016).
20. D. Yi, Ch. L. Flint, P. P. Balakrishnan, et al., PRL **119**, 077201 (2017).

Translated by K. Shakhlevich